Estimated Nitrogen Solubility and Phase Composition in Fe−13% Cr Steel after Its Additional Alloying with (Mn, Mo, V, Nb)

M. V. Kostina[a], *, L. G. Rigina[a, b], V. S. Kostina[a], A. E. Kudryashov[a], and R. S. Fedortsov[a]

[a] Baikov Institute of Metallurgy and Materials Science, Russian Academy of Sciences, Moscow, Russia
[b] Central Scientific Research Institute of Machine Building and Metalworking TsNIITMASh, Moscow, Russia
*e-mail: mvk@imet.ac.ru

Abstract—The solubility of nitrogen is estimated in Fe−13% Cr model steels of various compositions with additional alloying (by a small amount from several hundredths of a percent to 1.5%) with elements (Mn, Mo, V, Nb), which increase the solubility of nitrogen in iron-based solid solutions. 60 versions of compositions have been studied. Based on our earlier experimental data obtained for nitrogen-bearing steels with 16% Cr−5% Ni−Nb, we estimate the compositional stability coefficient of nitrogen K_s, which is used in the calculations of the nitrogen solubility, for martensitic steel. The calculated value of K_s is lower than that of austenitic steels. For steels of all composition versions with the calculated nitrogen content and various contents of additional alloying elements (Mn, Mo, V, Nb), their phase compositions are estimated using a modified Schaeffler−Delong diagram and a nonequilibrium Potak−Sagalevich diagram for steels heat treated to form a solid solution. All Fe−13% Cr−Mn, Mo, V, Nb compositions with a low carbon content (0.03−0.05%) at the maximum nitrogen concentration in a metal are shown to be in a martensite−ferrite region. The temperature of the onset of the martensitic transformation M_s is calculated using the empirical Finkler−Schirra formula, and a correlation between M_s and the ratio Ni_{eqiv}/Cr_{eqiv} (chromium and nickel equivalents calculated by the formulas used for the modified Schaeffler−Delong diagram) is revealed.

Keywords: steel, martensite, austenite, ferrite, nitrogen, carbon, phase transformations, Schaeffler−Delong diagram, Potak−Sagalevich diagram

DOI: 10.1134/S0036029523030060

INTRODUCTION

An analysis of the mechanical and corrosion properties of industrially produced and laboratory steels based on Fe−13% Cr after various types of heat treatment (HT) demonstrates that HT conditions are always a compromise between attempts to ensure strength, ductility, and corrosion resistance.[1] When the austenitizing temperature increases before quenching, the hardness of martensite-quenched steel increases as a result of the intensification of carbide dissolution of carbides: the higher the carbon content in steel, the higher the hardness [1−4]. Although quenched layers with 13% Cr have high corrosion resistance [5, 6], their use is limited because of the absence of plasticity. After quenching and low tempering at 200−300°C, these steels have a high strength, low plasticity [1, 2, 7−10], and rather good corrosion resistance [11−13], since a small amount of carbides precipitates at low tempering. The transition to a plas-

tic state, in which these steels have an acceptable impact toughness, is caused by the martensite−ferrite phase transformation during medium and high tempering at 500−750°C, when a significant amount of a carbide phase precipitates and its coagulation occurs [8−10]. However, the strength characteristics are relatively low in this case [8−10], and the corrosion resistance is worse than that after low tempering [11−13]. To improve the properties of these steels, HT conditions with double quenching and double tempering and HT with cooling to cryogenic temperatures [10, 14, 15] were tested; however, no properties fundamentally different from those after standard treatment were achieved. Therefore, investigations for searching for alternative treatment conditions are continuing. The first of them is a change in the phase composition and structure as a result of the so-called Q&P treatment (quenching and partitioning treatment) [16−19], which consists in quenching of steel to a temperature within the martensitic transformation range followed by its HT for carbon redistribution between formed martensite and untransformed austenite. The

---

[1] From here on, the element contents are given in wt %.

second version is the action of additional alloying on the properties of Fe−13% Cr steels [4, 20−22]. These methods are also combined to affect the structure and properties of Fe−13% Cr steels [23−26].

It is interesting to study the influence of nitrogen, as an interstitial element that substitutes for carbon or supplement it, on the properties of Fe−13% Cr steel. During HT, nitrogen introduced into chromium-containing steels instead of carbon forms CrN and Cr_2N chromium nitrides, which do not remove chromium from a solid solution in such large quantities removed by $Cr_{23}C_6$ carbides and do not form (upon alloying at equilibrium concentration) continuous nitride chains along grain boundaries (unlike these carbides). Nitrogen promotes noticeable solid-solution hardening and stabilizes austenite. The steels based on Fe−13% Cr and alloyed with nitrogen are poorly investigated [3, 16, 21, 26], the nitrogen content in these steels is usually low (0.02% [16], 0.08% [3]), and the contribution of nitrogen the properties of the steels is unclear. Only the authors of [26] present experimental data on Q&P treatment of steel with 13% Cr−0.258% C−0.166% N, which did not result in practically useful results. An alloy and steel with 13% Cr containing 0 and 0.14% C, respectively, with an overequilibrium nitrogen concentration of 0.24% (both manifested themselves as nonplastic materials) were investigated in [21].

The purpose of this work is to estimate the nitrogen solubility in Fe−13% Cr steels with various carbon contents and additionally alloyed with elements (Mn, Mo, V, Nb), which increase the solubility of nitrogen in iron-based solid solutions, and to calculate the phase composition (equilibrium and nonequilibrium) and the temperatures of the phase transformations involving austenite, ferrite, and martensite for steel compositions with the calculated nitrogen content.

EXPERIMENTAL

Material

The material to be studied is represented by model steels of various compositions based on Fe−13% Cr. Additional alloying elements (AE = Mn, Mo, V, Nb) were chosen with allowance for the well-known laws of their influence on the solubility of nitrogen (Fig. 1). Since silicon decreases the solubility of nitrogen (see Fig. 1), its content in the steels intended for nitrogen alloying should not be too high. Interstitial element carbon is known to decrease the solubility of nitrogen in steels, since its atoms occupy the same positions in the crystal lattice of austenite as nitrogen atoms do. We considered the following two approaches to choosing the carbon content: (1) the concept of maximum substitution of nitrogen for carbon (carbon is an impurity), which has been widely tested since the 1980s; (2) the physical concept of joint alloying of steels with carbon and nitrogen [28], which was proposed in the
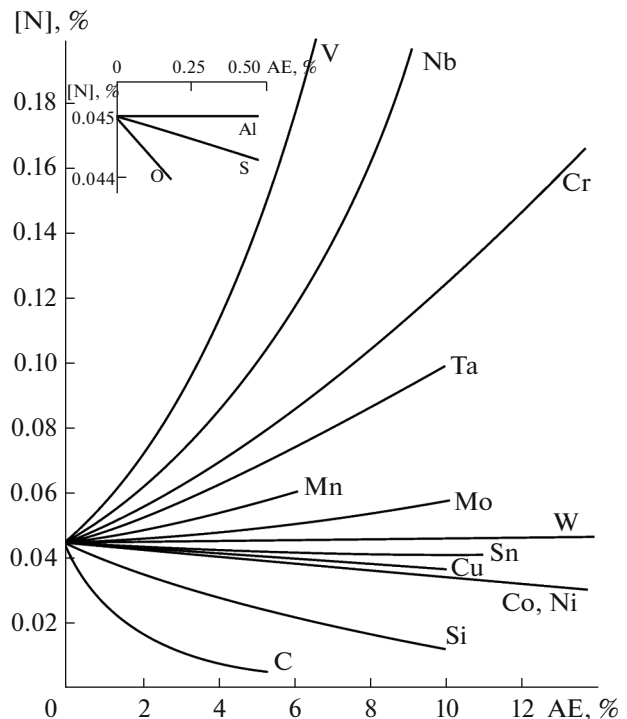

Fig. 1. Effect of the content of AE (see at the curves) on the equilibrium solubility of nitrogen in steels [27].

2000s on the basis of studying an electronic structure, atomic distribution, and thermodynamic stability. The metallic character of interatomic bonds reinforced by joint (C + N) alloying can be used to design high-strength corrosion-resistant steels with higher fracture energy; the ratio %C/%N ≈ 1 is considered effective.

Taking into account the solubility of nitrogen in Fe−13% Cr steels, we varied the contents of introduced AEs as follows: 0 and 1.5% Mn, 0 and 0.2% V, 0 and 0.07% Nb, and 0 and 0.5% Mo. The silicon content was selected at a level of 0.3%. The calculations were performed for the following 12 composition combinations: 1, Fe−13% Cr−N; 2, Fe−13% Cr−Mn−N; 3, Fe−13% Cr−Mn−Mo−N; 4, Fe−13% Cr−V−N; 5, Fe−13% Cr−Nb−N; 6, Fe− 13% Cr−V−Nb−N; 7, Fe−13% Cr−Mn−V−N; 8, Fe−13% Cr−Mn−Nb−N; 9, Fe−13% Cr−Mn−V−Nb−N; 10, Fe−13% Cr−Mo−V−N; 11, Fe−13% Cr−Mo−Nb−N; and 12−Fe−13% Cr−Mo−Nb−N. Each composition had five levels of carbon content: 0.03 (as an impurity), 0.15, 0.20, 0.25, and 0.30%. Composition 1 was used as a base for comparison. In total, 60 compositions were used in the calculations.

Calculation Methods

The formula for calculating the solubility of nitrogen was substantiated in detail in our work [29]. Here, we present the following formula for calculating the

Table 1. Comparison of the actual (N_{act}) and calculated ($[N]$)[1*] nitrogen contents and the calculated values of K_s coefficients for steels with 0.05% C−(14−16%) Cr−5% Ni−N, Nb[2*] according to our and literary [3, 25] data

No.	N_{fact}	[N]	$K_s = N_{fact}/[N]$	Content in steel, %					
	%			C	Cr	Ni	Mn	Si	Nb
1	0.13	0.195	0.635	0.040	16.25	5.36	0.40	0.54	0.07
2	0.10	0.192	0.52	0.054	15.5	4.62	0.06	0.1	−
3	0.15	0.194	0.785	0.058	15.3	4.63	0.07	0.1	−
4	0.18	0.212	0.928	0.088	15.5	4.65	0.07	0.1	−
5	0.15	0.205	0.71	0.068	15.8	2.38	0.06	0.1	−
6	0.17	0.204	0.83	0.028	15.75	4.25	0.43	0.27	0.06
7	0.14	0.206	0.68	0.027	15.72	4.15	0.39	0.29	0.075
8	0.16	0.176	0.68	0.033	16.1	4.7	0.48	0.48	0.075
9	0.15−0.18	0.195	0.94 (av.)	0.08−0.12	14.0−14.7	4.2−4.7	0.8−1.2	0.2−0.4	0.03−0.08
10	0.166[3*]	0.157	1.05	0.258	12.8	−	0.29	0.30	−
11	0.085[4*]	0.180	0.47	0.14	13.78	−	0.59	0.38	−

[1*] Calculation by Eq. (1).
[2*] Steels with ~14% Cr also contained 1.8−2.2% Mo and 0.3−0.5% Cu.
[3*] According to [25].
[4*] According to [3].

limiting nitrogen solubility [N] in a multicomponent melt:

$$\log[N] = -560/T - 1.06 - (2600/T - 0.39)$$
$$\times \{-0.048([Cr] + 0.5[Mn] - 2.45[C] - 0.9[Si]$$
$$- 0.23[Ni] + 0.27[Mo] + 2.04[V] - 0.12[Cu]$$
$$- 0.15[S] - [P]) + 3.5 \times 10^{-4}([Cr] + 0.5[Mn] \quad (1)$$
$$- 2.45[C] - 0.9[Si] - 0.23[Ni] + 0.27[Mo]$$
$$+ 2.04[V] - 0.12[Cu] - 0.15[S] - [P])^2$$
$$+ 0.13[N]\} + (700/T - 0.37) + 0.5\log p_{N_2}.$$

Formula (1) allows us to take into account the influence of temperature, pressure, and deviation from the Sieverts law and ensures the best agreement between the calculated and experimental results.

In the metallurgical practice of producing nitrogen-bearing steels, the concepts of compositionally stable nitrogen content (maximum possible content of this element in a solid defect-free metal) and compositional stability coefficient K_s are used. The latter characterizes the ratio of the nitrogen solubility limit in a metal under standard conditions to compositionally stable nitrogen content $[N]_{cs}$. Compositional stability coefficient K_s depends on the partial pressure of nitrogen above a melt, the chemical composition of the metal, and its phase composition in the solidus−liquidus temperature range ($T_S - T_L$). The compositionally stable nitrogen content is determined from the condition

$$[N]_{cs} = [N]K_s. \quad (2)$$

For austenitic chromium−nickel−manganese steels, researchers use an empirically determined com-

positional stability coefficient $K_s = 0.78$; for these steels, it is confirmed by the agreement between the calculated compositionally stable nitrogen content and the composition obtained for wrought and cast steels with 0.05% C−21% Cr−8% Ni−15% Mn—Mo, V, N studied in [30−32]. For these steels, the solubility of nitrogen was found to be 0.5% N. For duplex steels, we have $K_s = 0.45-0.5$; for iron, it is 0.28.

What is the level of K_s for Fe−13% Cr−based steels? We preliminarily estimated this coefficient using the few literature data available for Fe−13% Cr−based steels and the results of our earlier studies of steels with 0.05% C−(14−16%)Cr−(4−5%)Ni−N, Nb. The chromium content that promotes nitrogen dissolution is higher in the latter steels; however, in contrast to the former steels, they contain 4−5% Ni, which decreases the nitrogen solubility. These data are given in Table 1. Among the eleven values of K_s given in Table 1, two are very high ($K_s \approx 1$) and two are too low ($K_s \approx 0.5$). The average value of K_s according to our data is 0.75.

Literature sources showed the maximum [25] and minimum [3] values of K_s, and a nitrogen content that is higher than the calculated value at 100% assimilation was obtained in [25]. For the cases when the actual nitrogen contents in Table 1 correspond to the minimum value of K_s, we assume that the problem of reaching the maximum nitrogen content was not posed in steelmaking. On average, taking into account all the data, the value of K_s is at a level of 0.75. If all too high and too low values are not taken into account, its value is 0.72, which is lower than that for austenitic steels but higher than that for duplex steels. To estimate $[N]_{cs}$ by Eq. (2), we took $K_s = 0.72$.

Based on the calculated values of %N = $[N]_{cs}$, we estimated the influence of austenite- (Mn, C, N) and ferrite-forming (Mo, V, Nb) elements on the phase composition of the chosen compositions using a modified Schaeffler–Delong phase diagram. The phase composition was calculated using the modified Schaeffler–Delong diagram [33], in which the equivalents of austenite and ferrite formation are described by the following formulas:

$$Ni_{equiv} = Ni + 0.1Mn - 0.01Mn^2 \\ + 18N + 30C + 0.5Cu + 0.5Co, \quad (3)$$

$$Cr_{equiv} = Cr + 1.5Mo + 0.48Si + 2.3V \\ + 1.75Nb + 1.5Ti + 0.75W + 1.75Ta. \quad (4)$$

In Eqs. (3) and (4) and other calculation formulas, symbols AE = N, C, Si, Mn, Ni, Cr, Mo, V, Nb, W, Cu, Co, Ti, and Ta mean their content in steel, %.

In addition, the semi-quantitative structural diagram [34], which was developed for low-carbon corrosion-resistant steels and takes into account the influence of nitrogen and all the listed AEs on the austenite, martensite and ferrite contents in a structure, was used to estimate the phase composition of the steel. The mathematical approach to the phase composition calculation using this diagram is described in [35], where this diagram is presented with experimental results and our calculated data.

According to the Potak–Sagalevich diagram, the chromium equivalents of martensite (α) and ferrite (δ ferrite) formation are estimated using the AE content (%) by the formulas

$$Cr_{equiv}^{\alpha} = 20 - [Cr + 1.5Ni + 0.7Si + 0.75Mn \\ + K_{\alpha}(C + N) + 0.6Mo + 1.5V + 0.2Cu], \quad (5)$$

$$Cr_{equiv}^{\delta} = Cr - 1.5Ni + 2Si - 0.75Mn \\ - K_{\delta}(C + N) + Mo + 1.5V + 0.9Nb - 0.5Cu, \quad (6)$$

where K_{α} and K_{β} are the coefficients of influence of each AE on the martensite and ferrite formation, respectively.

In the Potak–Sagalevich diagram, the calculated values of Cr_{equiv}^{δ} are laid off along the abscissa axis, and the values of the resulting influence of AE on the chromium equivalent of martensite formation Cr_{equiv}^{α} (i.e., on the ratio of austenite γ to martensite α(M), which is determined by the γ → α transformation temperature) are laid off along the ordinate axis. The phase composition of steel is determined as the point of intersection of coordinates in the diagram.

As in the case of the Schaeffler diagram, the influence of each AE on both equivalents is normalized by a fixed coefficient with respect to chromium, but the values of coefficients K_{α} and K_{β} before the sum (C + N) in Eqs. (5) and (6) are variable and depend on the
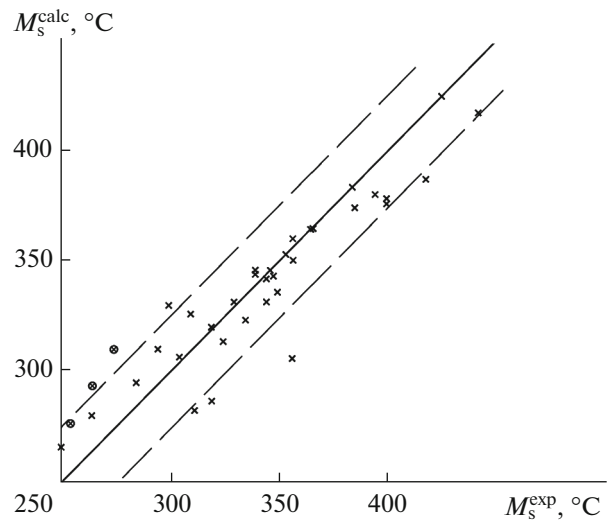

Fig. 2. Comparison of the experimental and calculated M_s temperatures for 38 steels based on 8–14% Cr with ~1 at % C, Mn, Ni, Mo, W, V [37].

total content of these elements in steel (see the inset to the Potak–Sagalevich diagram): $K_{\alpha} = 30$–35 and $K_{\delta} = 28$–31 at % C + %N = 0.17–≤0.30. If $Cr_{equiv}^{\delta} < 6$, ferrite is absent on the structure of steel; at $Cr_{equiv}^{\delta} \geq 6$, ferrite forms in steel; and at $Cr_{equiv}^{\alpha} \leq -4$, austenite begins to form.

The temperature of the onset of the martensitic transformation M_s was estimated using well-known empirical formulas. Handbook [36] with a database was used to calculate the critical temperatures of steel. After analyzing the conditions limiting the possibilities of applying certain calculations, we chose the Finkler and Schirra formula [37]

$$M_s = 635 - 474\{C + 0.86[N - 0.15(Nb + Zr)] \\ - 0.066(Ta + Hf)\} - (33Mn + 17Cr + 17Ni \quad (7) \\ + 21Mo + 39V + 11W).$$

Formula (7) results from studying 38 steels with a chromium content of 8–14% (Fig. 2) and the subsequent comparison of the experimental values of M_s temperatures with the calculated ones. The average deviation of the calculated and experimental temperatures of the onset of the martensitic transformation from the trend line described by Eq. (7) was found to be 25°C.

CALCULATION RESULTS

Summary Tables 2–6 present the results of calculating the compositionally stable nitrogen content calculated from the condition %N = $[N]_{cs} = 0.72[N]_{calc}$ and characterizing the solubility of nitrogen in the

Table 2. Estimation of the influence of Mn and Mo on $[N]_{cs}$ and the results of calculating the phase composition (according to the modified Schaeffler–Delong (Sh.–D.) diagram and the Potak–Sagalevich (P.–S.) diagram)* and the temperature of the onset of martensite formation upon cooling

Composition (see Figs. 3, 4)	%C	%Mn	%Mo	%N = $[N]_{cs}$	Ni_{equiv}	Cr_{equiv}	Sh.–D. phases	Cr_{equiv}^{δ}	Cr_{equiv}^{α}	P.–S. phases	M_S, °C
Fe−13% Cr−N	0.03	−	−	0.121	3.1	13.1	M + F	9.3	2.0	84% M + 16% F	351
	0.15	−	−	0.117	6.6	13.1	M	6.1	−1.7	98% M + 2% F/M	295
(1—●)	0.20	−	−	0.116	8.1	13.1	M	4.7	−3.2	M	272
	0.25	−	−	0.114	9.6	13.1	M/M + A	3.3	−4.7	92% M + 8% A	249
	0.30	−	−	0.113	11.1	13.1	M + A	2.0	−6.3	89% M + 11% A	226
Fe−13% Cr−Mn−N	0.03	1.5	−	0.130	3.4	13.1	M + F/M	8.0	0.6	92% M + 8% F	297
	0.15	1.5	−	0.126	6.9	13.1	M	4.7	−3.0	M	242
(2—●)	0.20	1.5	−	0.124	8.4	13.1	M	3.4	−4.6	93% M + 7% A	219
	0.25	1.5	−	0.123	9.9	13.1	M + A	2.0	−6.1	88% M + 12% A	196
	0.30	1.5	−	0.121	11.3	13.1	M + A	0.7	−7.6	86% M + 14% A	173
Fe−13% Cr−Mn−Mo−N	0.03	1.5	0.5	0.131	3.4	13.8	M + F	8.5	0.3	88% M + 12% F	286
	0.15	1.5	0.5	0.128	6.9	13.8	M	5.2	−3.4	M	231
(3—○)	0.20	1.5	0.5	0.126	8.4	13.8	M/M + A	3.8	−4.9	93% M + 7% A	208
	0.25	1.5	0.5	0.125	9.9	13.8	M + A	2.5	−6.4	92% M + 8% A	185
	0.30	1.5	0.5	0.123	11.4	13.8	M + A	1.1	−8.0	84% M + 16% A	162

* In Tables 2−6, Sh.−D. stands for the Schaeffler−Delong diagram and P.−S., for the Potak−Sagalevich diagram.

metal of 15 model compositions with five levels of carbon content (%C) and the results of calculating the phase composition and the phase transformation temperatures.

The results of calculating Ni_{equiv} and Cr_{equiv} and the corresponding phase composition of each composition are plotted on the enlarged area of the Schaeffler−Delong diagram (Fig. 3).

From the data in that part of Table 2 that reflects the effect of the AEs entering the solid solution (Cr, Mn, Mo) on the solubility of nitrogen, it follows that the calculated limit solubility of nitrogen in steel with 13% Cr and the minimum carbon content is 0.121%. It decreases when the carbon content increases. The introduction of 1.5% Mn leads to an increase in $[N]_{cs}$ to 0.13%. The addition of 0.5% Mo to manganese-
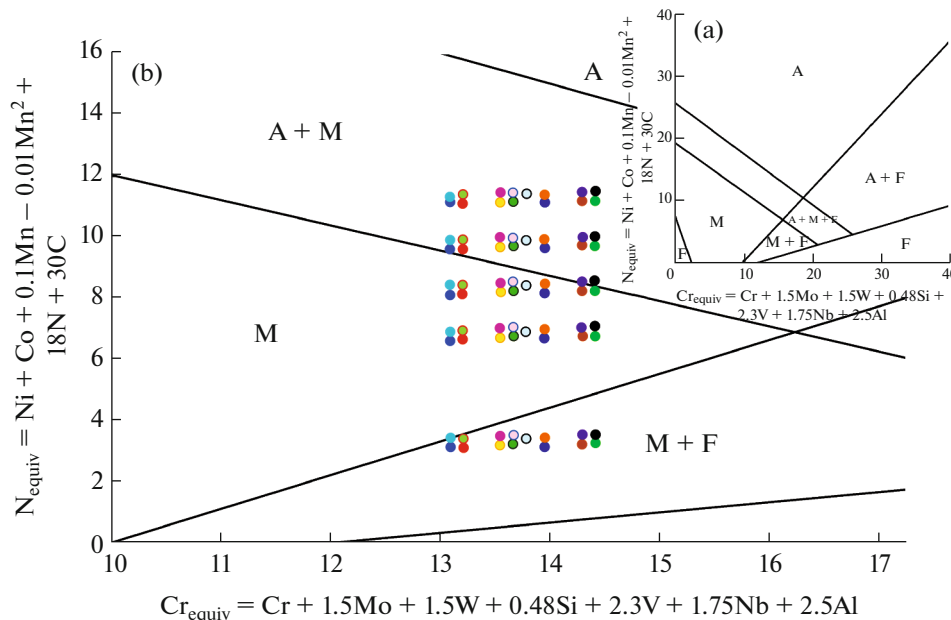

Fig. 3. Modified Schaeffler−Delong diagram: (a) general appearance (A is austenite; M, martensite; F, ferrite) and (b) enlarged region of the diagram with compositions 1−15 from Tables 2−6 ((●—1), (●—2), (○—3), (●—4), (●—5), (●—6); (●—7); (●—8); (○—9); (●—10); (●—11); (●—12); (●—13); (●—14); (●—15)).

Table 3. Estimation of the influence of V and Nb on $[N]_{cs}$ and the results of calculating the phase composition and the temperature of the onset of martensite formation upon cooling

Composition (see Figs. 3, 4)	%C	%V	%Nb	%N = $[N]_{cs}$	Ni_{equiv}	Cr_{equiv}	Sh.−D. phases	Cr^{δ}_{equiv}	Cr^{α}_{equiv}	P.−S. phases	M_S, °C
Fe−13% Cr−V−N (4—🟡)	0.03	0.20	–	0.126	3.19	13.56	M + F	9.6	1.7	81% M + 19% F	341
	0.15	0.20	–	0.122	6.72	13.56	M	6.5	−1.9	97% M + 3% F	285
	0.20	0.20	–	0.121	8.20	13.56	M/M + A	5.2	−3.3	M	262
	0.25	0.20	–	0.119	9.67	13.56	M + A	3.9	−4.8	93% M + 7% A	239
	0.30	0.20	–	0.118	11.14	13.56	M + A	2.6	−6.3	88% M + 12% A	216
Fe−13% Cr−Nb−N (5—🔴)	0.03	–	0.07	0.122	3.12	13.22	M + F	9.5	2.1	83% M + 17% F	355
	0.15	–	0.07	0.118	6.65	13.22	M	6.4	−1.4	98% M + 2% F	299
	0.20	–	0.07	0.117	8.13	13.22	M	5.1	−2.9	M	276
	0.25	–	0.07	0.115	9.60	13.22	M/M + A	3.7	−4.4	94% M + 6% A	253
	0.30	–	0.07	0.114	11.07	13.22	M	2.4	−5.9	90% M + 10% A	230
Fe−13% Cr−V−Nb−N (6—🟢)	0.03	0.20	0.07	0.127	3.21	13.68	M + F	9.7	1.7	81% M + 19% F	345
	0.15	0.20	0.07	0.123	6.74	13.68	M	6.5	−1.9	97% M + 3% F	289
	0.20	0.20	0.07	0.122	8.21	13.68	M/M + A	5.2	−3.4	M	276
	0.25	0.20	0.07	0.120	9.69	13.68	M + A	3.9	−4.8	93% M + 7% A	243
	0.30	0.20	0.07	0.119	11.16	13.68	M + A	2.6	−6.3	88% M + 12% A	220

Table 4. Estimation of the influence of Mn, V, and Nb on $[N]_{cs}$ and the results of calculating the phase composition and the temperature of the onset of martensite formation upon cooling

Composition (see Figs. 3, 4)	%C	%Mn	%V	%Nb	%N = $[N]_{cs}$	Ni_{equiv}	Cr_{equiv}	Sh.−D. phases	Cr^{δ}_{equiv}	Cr^{α}_{equiv}	P.−S. phases	M_S, °C
Fe−13% Cr−Mn−V−N (7—🟣)	0.03	1.5	0.20	–	0.135	3.48	13.56	M + F/M	8.4	0.4	90% M + 10% F	287
	0.15	1.5	0.20	–	0.131	7.01	13.56	M	5.3	−3.1	M	232
	0.20	1.5	0.20	–	0.130	8.48	13.56	M/M + A	4.0	−4.5	94% M + 6% A	219
	0.25	1.5	0.20	–	0.128	9.95	13.56	M + A	2.8	−6.0	89% M + 11% A	186
	0.30	1.5	0.20	–	0.126	11.42	13.56	M + A	1.5	−7.4	86% M + 14% A	163
Fe−13% Cr−Mn−Nb−N (8—🟢)	0.03	1.5	–	0.07	0.131	3.40	13.22	M + F/M	8.3	0.8	89% M + 11% F	301
	0.15	1.5	–	0.07	0.127	6.93	13.22	M	5.2	−2.6	M	246
	0.20	1.5	–	0.07	0.125	8.40	13.22	M	3.9	−4.1	94% M/M + 6% A	223
	0.25	1.5	–	0.07	0.124	9.88	13.22	M + A	2.6	−5.5	91% M + 9% A	200
	0.30	15	–	0.07	0.122	11.35	13.22	M + A	1.3	−7.0	87% M + 13% A	177
Fe−13% Cr−Mn−V−Nb−N (9—⚪)	0.03	1.5	0.20	0.07	0.136	3.50	13.68	M + F	8.4	0.4	88% M + 12% F	291
	0.15	1.5	0.20	0.07	0.132	7.03	13.68	M	5.4	−3.1	M	236
	0.20	1.5	0.20	0.07	0.130	8.50	13.68	M/M + A	4.1	−4.5	94% M + 6% A	213
	0.25	1.5	0.20	0.07	0.129	9.97	13.68	M + A	2.8	−6.0	90% M + 10% A	190
	0.30	1.5	0.20	0.07	0.127	11.44	13.68	M + A	1.5	−7.5	86% M + 14% A	167

alloyed steel increases the nitrogen content slightly. According to Table 3, it is possible to judge the effect of carbide- and nitride-forming elements (V, Nb) on the solubility of nitrogen. Vanadium is more effective, and the addition of niobium in an amount of 0.07% exerts a weak effect (it is this amount of niobium that is introduced into the nitrogen-bearing 05Kh16N5AB steels under study). As can be seen from Table 4, the combined introduction of manganese and vanadium makes it possible to achieve a nitrogen content of 0.135% in low-carbon steel. The calculated data of Table 5 demonstrate that simultaneous alloying with molybdenum, vanadium, and niobium gives the same

nitrogen solubility effect as the introduction of 1.5% Mn without the addition of other AEs (see Table 2). According to Table 6, the maximum solubility of nitrogen in low-carbon steel with the combined introduction of manganese, molybdenum, vanadium, and niobium reaches 0.138%.

Commenting on the data of Fig. 3 and Tables 2−6 in terms of calculating the phase composition of model compositions 1−15, we note the following division into groups of steels:

(i) All low-carbon compositions with 0.03% C fall into the ferrite region or at the boundary of an M + F/M phase mixture (compositions 7, 8).

Table 5. Estimation of the influence of Mo, V, and Nb on $[N]_{cs}$ and the results of calculating the phase composition and the temperature of the onset of martensite formation upon cooling

Composition (see Figs. 3, 4)	%C	%Mo	%V	%Nb	%N = $[N]_{cs}$	Ni_{equiv}	Cr_{equiv}	Sh.–D. phases	Cr^{δ}_{equiv}	Cr^{α}_{equiv}	P.–S. phases	M_s, °C
Fe−13% Cr−Mo−V−N	0.03	0.5	0.20	−	0.127	3.22	14.31	M + F	10.3	1.4	75% M + 25% F	276
(10—●)	0.15	0.5	0.20	−	0.124	6.75	14.31	M	7.2	−2.1	95% M + 5% F	221
	0.20	0.5	0.20	−	0.122	8.23	14.31	M/M + A	6.0	−3.5	99% M + 1% F/M	198
	0.25	0.5	0.20	−	0.121	9.70	14.31	M + A	4.7	−5.0	93% M + 7% A	175
	0.30	0.5	0.20	−	0.119	11.17	14.31	M + A	3.4	−6.4	88% M + 12% A	152
Fe−13% Cr−Mo−Nb−N	0.03	0.5	−	0.07	0.123	3.15	13.97	M + F	10.1	1.8	78% M + 22% F	290
(11—●)	0.15	0.5	−	0.07	0.120	6.68	13.97	M	7.1	−1.7	96% M + 4% F	235
	0.20	0.5	−	0.07	0.118	8.15	13.97	M/M + A	5.8	−3.1	M	212
	0.25	0.5	−	0.07	0.117	9.63	13.97	M + A	4.6	−4.6	93% M + 7% A	189
	0.30	0.5	−	0.07	0.115	11.10	13.97	M + A	3.3	−6.0	90% M + 10% A	166
Fe−13% Cr−Mn−Mo−V−Nb−N	0.03	0.5	0.20	0.07	0.128	3.24	14.43	M + F	10.3	1.4	75% M + 25% F	334
(12—●)	0.15	0.5	0.20	0.07	0.125	6.77	14.43	M	7.3	−2.1	94% M + 6% F	278
	0.20	0.5	0.20	0.07	0.123	8.24	14.43	M/M + A	6.0	−3.6	99% M + 1% F/M	255
	0.25	0.5	0.20	0.07	0.122	9.72	14.43	M + A	4.7	−5.0	93% M + 7% A	232
	0.30	0.5	0.20	0.07	0.120	11.19	14.43	M + A	3.5	−6.5	88% M + 12% A	209

Table 6. Estimation of the influence of Mn, Mo, V, and Nb on $[N]_{cs}$ and the results of calculating the phase composition and the temperature of the onset of martensite formation upon cooling

Composition (see Figs. 3, 4)	%C	%Mn	%Mo	%V	%Nb	%N = $[N]_{cs}$	Ni_{equiv}	Cr_{equiv}	Sh.–D. phases	Cr^{δ}_{equiv}	Cr^{α}_{equiv}	P.–S. phases	M_s, °C
Fe−13% Cr−Mn−Mo−V−N	0.03	1.5	0.5	0.20	−	0.137	3.51	14.31	M + F	8.9	0.1	86% M + 14% F	276
(13—●)	0.15	1.5	0.5	0.20	−	0.133	7.04	14.31	M	5.9	−3.4	M	221
	0.20	1.5	0.5	0.20	−	0.131	8.51	14.31	M/M + F	4.7	−4.9	93% M + 7% A	198
	0.25	1.5	0.5	0.20	−	0.130	9.98	14.31	M + A	3.4	−6.3	88% M + 12% A	175
	0.30	1.5	0.5	0.20	−	0.128	11.45	14.31	M + A	2.1	−7.8	84% M + 16% A	152
Fe−13% Cr−Mn−Mo−Nb−N	0.03	1.5	0.5	−	0.07	0.132	3.43	13.97	M + F	8.8	0.5	87% M + 13% F	290
(14—●)	0.15	1.5	0.5	−	0.07	0.129	6.96	13.97	M	5.8	−3.0	M	235
	0.20	1.5	0.5	−	0.07	0.127	8.43	13.97	M/M + A	4.5	−4.4	93% M + 7% A	212
	0.25	1.5	0.5	−	0.07	0.125	9.91	13.97	M + A	3.3	−5.9	90% M + 10% A	189
	0.30	1.5	0.5	−	0.07	0.124	11.38	13.97	M + A	2.0	−7.4	86% M + 14% A	166
Fe−13% Cr−Mn−Mo−V−Nb−N	0.03	1.5	0.5	0.20	0.07	0.138	3.53	14.43	M + F	9.0	0.0	86% M + 14% F	287
(15—●)	0.15	1.5	0.5	0.20	0.07	0.134	7.06	14.43	M	6.0	−3.5	99% M + 1% F/M	232
	0.20	1.5	0.5	0.20	0.07	0.132	8.53	14.43	M + A	4.7	−4.9	92% M + 8% A	208
	0.25	1.5	0.5	0.20	0.07	0.131	10.00	14.43	M + A	3.4	−6.4	88% M + 12% A	179
	0.30	1.5	0.5	0.20	0.07	0.129	11.47	14.43	M + A	2.2	−7.8	84% M + 16% A	156

(ii) All compositions with 0.15% C fall in the martensite region.

(iii) Depending on the ratio Ni_{equiv}/Cr_{equiv}, compositions with 0.20% C are either in the martensitic region near the M/M + A phase boundary or at this boundary. In practice, this means that retained austenite can exist in such steels under certain HT conditions. According to the calculation, only one of the 15 considered versions with 0.20% C has a martensitic−austenitic structure (near phase region boundary): this is steel with the maximum AE content increasing the solubility of nitrogen (see Fig. 3 and Table 6).

(iv) All compositions with 0.25 and 0.30% C have a martensitic−austenitic structure except for the composition with 0.25% C without additional AEs (Mn, Mo, V, Nb).

The results of calculating the phase composition according to the Schaeffler−Delong (see Fig. 3) and Potak−Sagalevich (Fig. 4) diagrams are quite close (see Tables 2−6). However, from a comparison of Figures 3 and 4, it is clearly seen that the calculations using the Potak−Sagalevich diagram gives a noticeably smaller number of compositions in the martensitic region and a larger number of compositions in the austenitic−ferritic and austenitic−martensitic regions.
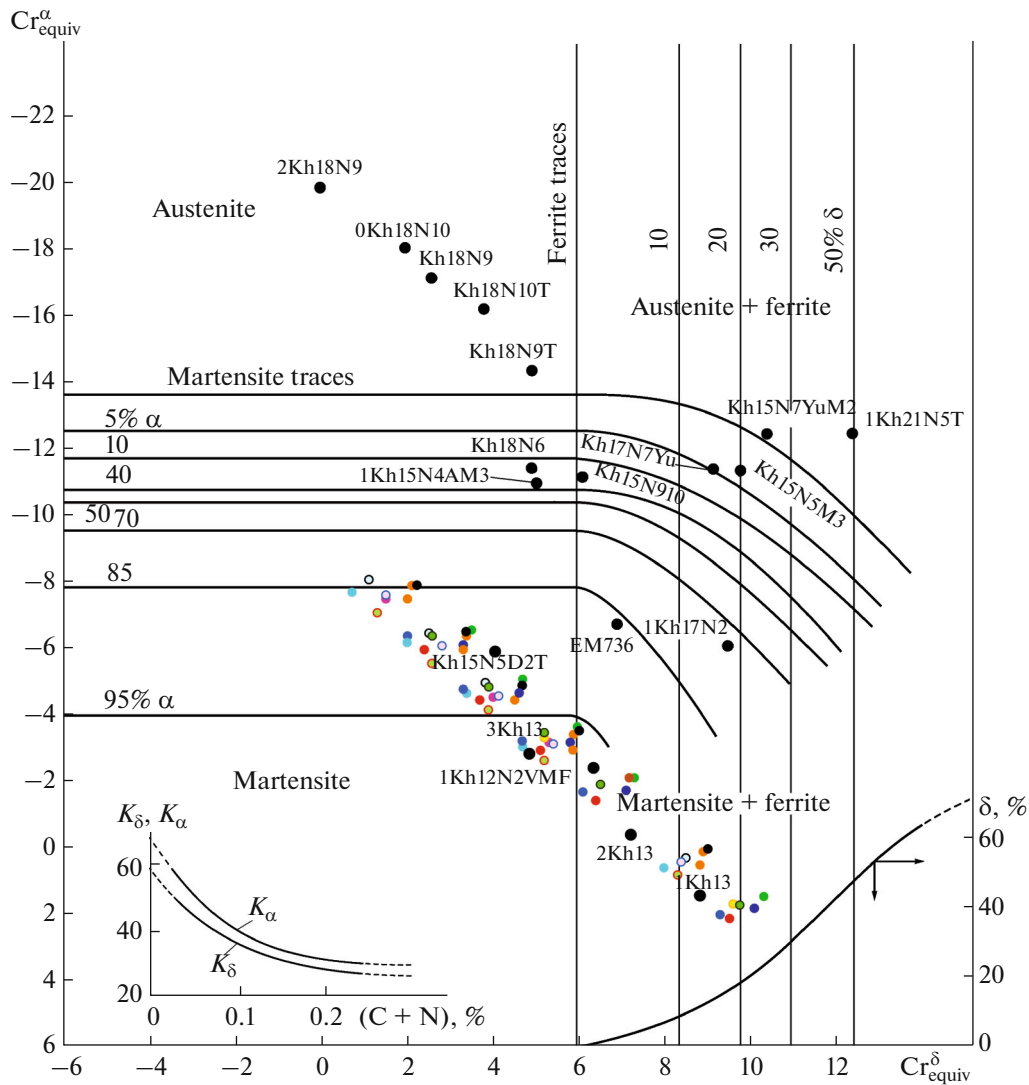
Fig. 4. Structural Potak−Sagalevich diagram for wrought corrosion-resistant steels (after solution treatment annealing) [35] with the calculation region covering compositions 1−15 from Tables 2−6 with calculated nitrogen content %N = [N]$_{cs}$. α is martensite; δ, ferrite. Note: The steel grades indicated in the diagram are now designated with a difference related to information about carbon content. For example, 1Kh13 and 2Kh13 steels with 0.10 and 0.20% carbon, respectively, presented in the diagram are now designated as 10Kh13 and 20Kh13, respectively.

According to the Potak−Sagalevich diagram, model compositions with 0.15% C, namely, compositions 1 (see Table 2), 4, 5, 6 (see Table 3), 10, 11, 12 (see Table 5) and 15 (see Table 6), are located in the martensitic−ferritic region (see Fig. 4). The martensite content in them ranges from ~94 to 98%. At the same time, these compositions in the Schaeffler−Delong diagram turn out to be completely in the martensitic region.

The calculated phase composition of the model steels of compositions 2 and 8 (0.20% C) and composition 5 (0.30% C) in the Schaeffler−Delong diagram is in the martensitic region, and those in the Potak−Sagalevich diagram are in the martensitic−austenitic region with 6−10% retained austenite (see Figs. 3, 4). Austenite should be present in phase compositions 4, 6, and 11 with 0.20% C according to the Schaeffler−Delong diagram (see Fig. 3), and these compositions in the Potak−Sagalevich diagram are located in an area with a 100% martensitic structure. The phase compositions of all model steels included in compositions 10 and 12 with 0.20% C are in the M + A region in the Schaeffler−Delong diagram and in the M + F region in the Potak−Sagalevich diagram. However, for compositions with 0.20% C included in composition 13, the reverse picture is observed: the Schaeffler−Delong diagram predicts an M + F phase composition, and
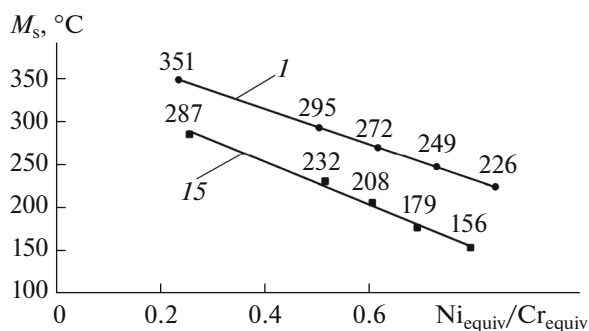
M_s, °C

Fig. 5. Temperature of the onset of the martensitic transformation M_s vs. the ratio Ni_{eqiv}/Cr_{eqiv} for steels of compositions 1 and 15 from Tables 2 and 6, respectively: (*1*) Fe−13% Cr−N composition and (*15*) Fe−13% Cr−Mn−Mo−V−Nb−N composition.

these steels in the Potak−Sagalevich diagram should be in the M + A region.

The calculated temperatures of the onset of the martensitic transformation (M_s) for all compositions 1−15 are also given in Tables 2−6. An attempt was made to estimate to what extent the calculated M_s temperatures correlate with the ratio Ni_{eqiv}/Cr_{eqiv} calculated by Eqs. (3) and (4). For this estimation, we used the M_s temperatures of the steels included in compositions 1 (Fe−13% Cr−N) and 15 (Fe−13% Cr−Mn−Mo−V−Nb−N) in Tables 2 and 6, i.e., the least and most alloyed model steels based on Fe−13% Cr. In both cases, the calculated M_s points formed linear dependences (Fig. 5):

for the steels of composition 1,

$$M_s = -206.1(Ni_{equiv}/Cr_{equiv}) + 398.8; \qquad (8)$$

for the steels of composition 15,

$$M_s = -248.4(Ni_{equiv}/Cr_{equiv}) + 354.1. \qquad (9)$$

Within each composition, this temperature decreases with increasing carbon content. An increase in the ratio Ni_{eqiv}/Cr_{eqiv} and an increase in the total content of additional AEs leads to a decrease in M_s. The values of M_s for the steels of compositions 2−14 are located within the band bounded by the lines for compositions 1 and 15 in Fig. 5.

DISCUSSION
Nitrogen Solubility Calculations

The authors of [38], proposed a formula for calculating the solubility of nitrogen and presented data on the theoretical solubility of nitrogen at 1600°C implemented in practice for steels with ~8, 11, 15, 17, and 20% Cr, from 0.096 to 0.22% C, from 0.36 to 1.16% Si, and microalloyed by Mo, V, Nb, and Cu. Our version of calculation for the melt compositions from [38] with 8 and 10% Cr gives values of [N], which differ

from the data in [38] only by several thousandths of a percent. For higher chromium contents, the discrepancy increases: our calculations give a higher value of [N]. For example, for heat M5 of steel with 15.43% Cr from [38], our calculation gives [N] = 0.208% and the compositionally stable nitrogen content is $[N]_{cs}$ = 0.150%, whereas the theoretical solubility in [38] is 0.124% and the actual content is 0.161%, i.e., above our calculated value of $[N]_{cs}$. However, this excess led to the appearance of gas pores in the heat M5 ingot [38]. Earlier, we achieved a nitrogen content of 0.15% in steel with 15% Cr (see Table 1). Thus, for steel with 13% Cr, our version of the formula for estimating the limiting solubility of nitrogen seems to be close to that to be used in practice. As was noted in [39] more nitrogen dissolves in the melt of martensitic corrosion-resistant steel if the carbon content increases at normal pressure, since the fraction of ferrite decreases during solidification.

Phase Composition Calculations

In the case of a less optimistic forecast on the limiting solubility of nitrogen for the compositions considered in our work, all calculation points shift: martensitic steel with retained austenite moves toward the martensitic region and so on. Note that, in practice, it is possible to implement the schemes involving cryogenic treatment, thermomechanical treatment, and Q&P treatment [18, 40−42], after which the phase composition of the alloy can change in comparison with that predicted according to the diagrams. It is also important to take into account that the structure and phase composition of Fe−13% Cr family steels with different carbon concentrations are determined by a large number of factors (temperature and time of holding in the austenitic region, heating rate, cooling rate from the austenitic region; variations in tempering mode parameters) affecting the type and morphology of carbides, their dissolution and precipitation, and the phase transformations involving ferrite, martensite, and austenite.

In all considered steels with nitrogen, low-carbon steel (with 0.03% C) falls into the martensitic−ferritic region. Using steel with <0.2% C and 13% Cr, which is used for casing pipes [8], as an example, we can use our calculation technique to estimate how a small addition of nitrogen can affect the phase composition of the steel. This steel in the Potak−Sagalevich diagram is in the martensitic−ferritic region and can contain about 10% ferrite in the quenched state at 0.18% C; for the calculations using the modified Schaeffler−Delong diagram, this steel is in the martensitic region. At 0.11% N (below the maximum calculated solubility for this steel), this same steel in the Potak−Sagalevich diagram should be completely martensitic; in the second diagram, it shifts toward higher values of Ni_{equiv}. The authors of [8] note that, after quenching from

975°C, this steel is characterized by the presence of lath martensite and a hardness of 525 HV.

M_s Calculations and Dependences $M_s = f(Ni_{eqiv}/Cr_{eqiv})$

Formula (7) [37] (used since 1986) chosen by us for M_s calculation was obtained by processing a sufficiently large experimental body of experiments. The use of Eqs. (3) and (4) for calculating Ni_{eqiv} and Cr_{eqiv} has proven itself well enough. They are the product of several decades of evolution of the initial Schaeffler diagram [43] created in 1949 to evaluate the phase composition of the welded joints of corrosion-resistant steels. (In 1977, Delong added element nitrogen with a coefficient of 30 to the basic formula for calculating Ni_{eqiv} [44]. In 1999, Uggowitzer et al. [33] modified the Schaeffler–Delong diagram: the coefficients before the nitrogen and manganese contents were decreased for Ni_{eqiv}, and the formula for calculating Cr_{eqiv} was changed.) Therefore, it is noteworthy, but not surprising that the values of M_s calculated by Eq. (7) (see Fig. 5) linearly depend on the ratio Ni_{eqiv}/Cr_{eqiv} calculated by Eqs. (3) and (4). In fact, such consistency of the calculations obtained on the basis of different arrays of independent experimental studies is their additional mutual verification. It provides the possibility of a preliminary rough estimation of the M_s temperature, which can be convenient for choosing a technology of deformation and heat treatment and is especially important if we are talking about Q&P treatment including incomplete quenching and subsequent annealing to redistribute carbon between retained austenite and martensite. Especially for Fe–13% Cr steels, a comparison of conventional quenching and tempering with Q&P treatment confirms a significantly increased strength of materials combined with good ductility in the latter case [41], while the deformability remains acceptable [42].

CONCLUSIONS

(1) We calculated the limiting solubility of nitrogen in 60 model compositions based on Fe–13% Cr (hereafter, the element contents are in wt %) with 0.3% Si, five levels of carbon content (0.03, 0.15, 0.20, 0.25, 0.30%), and varying contents of Mn (0, 1.5), V (0, 0.2), Nb (0, 0.07), and Mo (0, 0.5). For calculations, we used a formula, which takes into account the influence of temperature, pressure, and deviation from the Sieverts law and exhibited the best agreement between the calculated and experimental results at a compositional stability coefficient of 0.72 calculated in this work. The maximum calculated nitrogen contents ranged from 0.113 to 0.138% depending on the influence of the content of alloying elements specified in the calculation model.

(2) Steels with the maximum calculated nitrogen content are characterized by the following:

(i) all low-carbon compounds with 0.03% C fall into the ferrite F region or at the boundary of a mixture M + F/M;

(ii) all compositions with 0.15% C fall into the martensite M region;

(iii) depending on the ratio Ni_{eqiv}/Cr_{eqiv}, compositions with 0.20% C are either in the martensitic region near the M/M + A boundary or at this boundary;

(iv) all compositions with 0.25 and 0.30% C have a martensitic–austenitic structure except for a composition with 0.25% C not additionally alloyed with Mn, Mo, V, and Nb.

(3) The calculations of the temperature of the onset of the martensitic transformation using the empirical Finkler–Schirra formula demonstrated a correlation between the M_s temperature and the ratio Ni_{eqiv}/Cr_{eqiv} (chromium and nickel equivalents were calculated using the formulas for the modified Schaeffler–Delong diagram).

(4) For minimally and maximally alloyed compositions based on Fe–13% Cr–N and Fe–13% Cr–Mn–Mo–V–Nb–N with five different levels of carbon content, the following dependences were obtained: $M_s = -206.1(Ni_{eqiv}/Cr_{eqiv}) + 398.8$ and $M_s = -248.4(Ni_{eqiv}/Cr_{eqiv}) + 354.1$, respectively.

CONFLICT OF INTEREST

The authors declare that they have no conflicts of interest.

REFERENCES

1. V. V. Ivashko, "Influence of heating conditions on the structure and properties of 20Kh13 stainless steel," Vestn. BarGU. Ser. Tekh. Nauki, No. 3, 45–48 (2015).

2. C. J. Scheuer, R. A. Fraga, R. P. Cardoso, and S. F. Brunatto, "Effects of heat treatment conditions on microstructure and mechanical properties of AISI 420 steel," in *Proceedings of 21 CBECIMAT—Congresso Brasileiro de Engenharia e Ciência dos Materiais 09 (Cuiaba, 2014)*, pp. 5857–5867.

3. Xiao Li and Yinghui Wei, "Effect of austenitizing heat treatment on microstructure and properties of a nitrogen bearing martensitic stainless steel," Open Phys. **17**, 601–606 (2019).
https://doi.org/10.1515/phys-2019-0061

4. C. Garcia de Andrés, L. F. Álvarez, and V. López, "Effects of carbide-forming elements on the response to thermal treatment of the X45Cr13 martensitic stainless steel," J. Mater. Sci. **33**, 4095–4100 (1998).
https://doi.org/10.1023/A:1004424329556

5. I. Bösing, L. Cramer, M. Steinbacher, W. Zoch, J. Thöming, and M. Baune, "Influence of heat treatment on the microstructure and corrosion resistance of

martensitic stainless steel," AIP **9**, 065317 (2019).
https://doi.org/10.1063/1.5094615

6. P. Rosemann, C. Müller, N. Kauss, and T. Halle, "Einfluss der Wärmebehandlung auf Mikrostruktur und Korrosionsverhalten kohlenstoffhaltiger nichtrostender stähle," https://www.researchgate.net/publication/281243566.

7. B.-A. Behrens, S. Hübner, C. Sunderkötter, L. Gebel, S. Gnaβ, G. Berndt, C. Trimborn, and C. Pfeffer, "Influence of process parameters on the hot stamping of carbon-martensitic chromium steel sheets," IOP Conf. Series: Mater. Sci. Eng. **418**, 012007 (2018).
https://doi.org/10.1088/1757-899X/418/1/012007

8. Ma Hou-Yu, He Yin-Sheng, Lee Kwon-Yeong, and Shin Keesam, "Effect of heat treatment on microstructural evolution of 13Cr martensitic stainless steel," Key Eng. Mater. Submitted **727**, 29—35 (2016).
https://doi.org/10.4028/www.scientific.net/ KEM.727.29

9. https://www.rodacciai.com/UPLOAD/datasheets/420B_X30Cr13-Nr.1.4028-ENG.pdf.

10. A. K. F. Hassan and Q. A. Jawad, "Investigation of the effect of austenitizing temperature and multiple tempering on the mechanical properties of AISI 410 martensitic stainless steel," The Iraqi J. Mechan. Mater. Eng. Special Volume Babylon First Intern. Eng. Conf. C, 411—435 (2016).

11. S. K. Bonagani, V. Bathula, and V. Kain, "Influence of tempering treatment on microstructure and pitting corrosion of 13 wt % Cr martensitic stainless steel," Corros. Sci. **131**, 340—354 (2018).
https://doi.org/10.1016/j.corsci.2017.12.012

12. Lu Si-Yuan, Yao Ke-Fu, Chen Yun-Bo, Wang Miao-Hui, Liu Xue, and Ge Xueyuan, "The effect of tempering temperature on the microstructure and electrochemical properties of a 13 wt % Cr-type martensitic stainless steel," Electrochim. Acta **165**, 45—55 (2015).
https://doi.org/10.1016/j.electacta.2015.02.038.

13. Y. Zhou and D. L. Engelberg, "Accessing the full spectrum of corrosion behaviour of tempered type 420 stainless steel," Mater. Corros. **72** (11), 1718—1729 (2021).
https://doi.org/10.1002/maco.202112442

14. S. Kulkarni, P. Srinivas, P. K. Biswal, G. Balachandran, and V. Balasubramanian, "Improvement in mechanical properties of 13Cr martensitic stainless steels using modified heat treatments," in *Proceedings of 28th ASM Heat Treating Society Conference* (Detroit, 2015), 335—341 (2015).

15. S. H. Mohamed, A. H. Ataiwi, J. J. Dawood, "Mechanical properties of martensitic stainless steel (AISI420) subjected to conventional and cryogenic treatments," Eng. Technol. J. A **38** (8), 1096—1105 (2020).
https://doi.org/10.30684/etj.v38i8A.517

16. S. Dieck, M. Ecke, T. Halle, and P. Rosemann, "Improvement of the martensitic stainless steel X46Cr13 by Q&P heat treatment," Symp. Mater. Join. Technol. IOP Conf. Series: Mater. Sci. Eng. **882**, 012006 (2020).
https://doi.org/10.1088/1757-899X/882/1/012006

17. Si-Yuan Lua, Ke-Fu Yaoa, Yun-Bo Chen, Miao-Hui Wang, Na Chena, and Xue-Yuan Ge, "Effect of quenching and partitioning on the microstructure evolution and electrochemical properties of a martensitic stainless steel," Corros. Sci. **103** (February), 95—104 (2016).
https://doi.org/10.1016/j.corsci.2015.11.010

18. Eunjung Seo and Bruno C. De Cooman, "Quenching and partitioning (Q&P) processing of AISI 420 stainless steel," in *Proceedings of the 8th Pacific Rim International Congress on Advanced Materials and Processing* (Springer, Cham., 2013), pp. 809—817.
https://doi.org/10.1007/978-3-319-48764-9_100

19. J. Mola and B. C. De Cooman, "Quenching and partitioning (Q&P) processing of martensitic stainless steels," Metall Mater. Trans. A **44**, 946—967 (2013).
https://doi.org/10.1007/s11661-012-1420-1

20. Weijian Liu, Jing Li, Shouhui Li, and Xuejun Li, "Effect of nitrogen on the hot deformation behavior of 0.4C—13Cr martensitic stainless steel," Steel Res. Int. **92**, (2021).
https://doi.org/10.1002/srin.202100020

21. G. M. Grigorenko, Yu. M. Pomarin, V. V. Lakomskii, V. Yu. Orlovskii, and I. I. Alekseenko, "Properties of nitrogen-alloyed Kh13-type steels," Obshch. Vopr. Metallurg., No. 4, 26—29 (2010).

22. Yiwei Zhang, Yuande Yin, Diankai Li, Ping Ma, Qingyun Liu, Xiaomin Yuan, and Shengzhi Li, "Temperature dependent phase transformation kinetics of reverted austenite during tempering in 13Cr supermartensitic stainless steel," Metals **9** (11), 1203 (2019).
https://doi.org/10.3390/met9111203

23. Junya Tobata, Kinh-Luan Ngo-Huynh, Nobuo Nakada, Toshihiro Tsuchiyama, and Setsuo Takaki, "Role of silicon in quenching and partitioning treatment of low-carbon martensitic stainless steel," ISIJ Int. **52** (7), 1377—1382 (2012).
https://doi.org/10.2355/isijinternational.52.1377

24. S. V. Ruschchits, A. M. Akhmed'yanov, A. N. Makovetskii, and A. O. Krasnotalov, "Quenching with subsequent carbon enrichment of untransformed austenite (Q&P treatment) of martensitic corrosion-resistant AISI 414 steel," Vestn. YuUrGU. Ser. Metallurg. **18** (4), 89—97 (2018).
https://doi.org/10.14529/met180410

25. Qiuliang Huang, C. Schröder, H. Biermann, O. Volkova, and J. Mola, "Influence of martensite fraction on tensile properties of quenched and partitioned (Q&P) martensitic stainless steels," Steel Res. Int. **87** (8) (2016).
https://doi.org/10.1002/srin.201500472

26. S. Jenicek, I. Vorel, J. Kana, K. Opatova, K. Rubesova, V. Kotesovec, and B. Masek, "Evolution of microstructure and mechanical properties during Q&P processing of medium carbon steels with different silicon levels," IOP Conf. Ser.: Mater. Sci. Eng. **18**, 012035 (2017).
https://doi.org/10.1088/1757-899X/181/1/012035

27. R. D. Pehlke and J. F. Elliott, Trans. AIME **218**, 1088 (1960).

28. V. G. Gavriljuk, B. D. Shanina, and H. Berns, "A physical concept for alloying steels with carbon + nitrogen," Mater. Sci. Eng. A **481/482** (May), 707—712 (2008). (Proceedings of the 7th European Symposium on Martensitic Transformations, ESOMAT 2006).
https://doi.org/10.1016/j.msea.2006.11.186

29. M. V. Kostina and L. G. Rigina, "Nitrogen-bearing steels and methods of their production," Izv. Vyssh. Uchebn. Zaved., Chern. Metall. **63** (8), 606−622 (2020).
https://doi.org/10.17073/0368-0797-2020-8-606-622

30. V. M. Blinov, O. A. Bannykh, M. V. Kostina, L. G. Rigina, and E. V. Blinov, "Effect of alloying on the limiting solubility of nitrogen in corrosion-resistant low-carbon Fe−Cr−Mn−Ni−Mo alloys," Metally, No. 4, 42−49 (2004).

31. M. V. Kostina, L. G. Rigina, O. A. Bannykh, B. M. Blinov, and S. O. Muradyan, "Development of a new cast highly corrosion-resistant and high-strength austenitic steel alloyed with nitrogen. Part 2. Investigation of the effect of alloying on the compositionally stable nitrogen content and phase composition after solidification of corrosion-resistant Fe−Cr−Mn−Ni−Mo−V−Nb alloys," Zagotovit. Proizv. Mashinostr., No. 4, 30−38 (2011).

32. A. A. Sisev, S. G. Tsimerman, M. V. Kostina, A. I. Il'inskii, M. M. Perkas, and L. G. Rigina, "Development of industrial technology of plasma-arc remelting of nitrogen-bearing 05Kh21AG15N8MF steel," Elektrometallurgiya, No. 12, 3−11 (2017).

33. P. J. Uggowitzer, W.-F. Bähre, H. Wohlfromm, and M. O. Speidel, "Nickel-free high nitrogen austenitic stainless steels produced by metal injection moulding," Mater. Sci. Forum. Switzerland **318−320**, 663−672 (1999).
https://doi.org/10.4028/www.scientific.net/MSF.318-320.663

34. Ya. M. Potak and E. A. Sagalevich, "Structural diagram of wrought stainless steels," Metalloved. Term. Obrab. Met., No. 9, 12−16 (1971).

35. G. S. Krivonogov and E. N. Kablov, "Mathematical model of the structural diagram of low-carbon corrosion-resistant steels and its application in the development of new materials," Metally, No. 5, 42−48 (2001).

36. A. Gorni, *Steel Forming and Heat Treating Handbook* (Sao Vicente SP Brazil, 2019).
https://doi.org/10.13140/RG.2.1.1695.9764

37. H. Finkler and M. Schirra, "Transformation behavior of high temperature martensitic steels with 8 to 14% chromium," Steel Res. **67** (8), 328−336 (1986).

38. V. Valasamudram and J. Anburaj, "Attainment of nitrogen solubility, characteristic study and its effects on martensitic stainless steel using conventional method of melting in as cast condition," Int. J. Eng. Technol. **7** (2.24), 588−591 (2018).

39. N. Krasokha and H. Berns, "Study on nitrogen in martensitic stainless steels," HTM J. Heat Treat. Mater. **66** (3), 150−164 (2011).
https://doi.org/10.3139/105.110099

40. S. C. Krishna, N. K. Karthick, A. K. Jha, Bhanu Pant, and P. V. Venkitakrishnan, "Microstructure and properties of nitrogen-alloyed martensitic stainless steel," Metallogr. Microstruct. Anal. **6**, 425−432 (2017).
https://doi.org/10.1007/s13632-017-0381-6

41. Xiao Li, Lifeng Hou, Yinghui Wei, and Zhengyan Wei, "Constitutive equation and hot processing map of a nitrogen-bearing martensitic stainless steel," Metals **10** (11), 1502 (2020).
https://doi.org/10.3390/met10111502

42. H. Altenbach, M. Brünig, and Z. L. Kowalewski, "Advanced structured materials," Plasticity, Damage and Fracture in Advanced Materials **121** (2020).
https://doi.org/10.1007/978-3-030-34851-9

43. A. L. Schaeffler, "Constitution diagram for stainless steel weld metal," Met. Prog. **56** (11), 680−681 (1949).

44. W. T. Delong, "Ferrite in austenitic stainless steel weld metal," Weld. Res. Supp. **53**, 273−286 (1974).

Translated by K. Shakhlevich